2008 IEEE International Conference on
Robotics and Automation
Pasadena, CA, USA, May 19-23, 2008

Underactuated Virtual Passive Dynamic Walking with an Upper Body

Fumihiko Asano and Zhi-Wei Luo

Abstract— **Achieving energy-efficient dynamic walking has become one of the main subjects of research on robotic bipedal locomotion. Approaches based on passive-dynamic walkers can accomplish bipedal locomotion. However, passive dynamic walking has only been studied with the legs, and the effect of an upper body has not been clarified. This paper investigates the effect of an upper body on the efficiency and stability of dynamic bipedal locomotion based on observations. We first investigated a suitable upper body, which was a simple 1-link torso with a bisecting hip mechanism that would not destroy natural dynamics of the biped model. Second, we analyzed the robot's driving mechanism and chose underactuated virtual passive dynamic walking as the method for generating an efficient dynamic gait. We confirmed that efficient dynamic walking was possible with a specific resistance of 0.01 and investigated the effect of the physical parameters of the upper body through numerical simulations.**

I. INTRODUCTION

Passive-dynamic walkers are good examples of energy-efficient dynamic walking [1]. They generally have only leg links and no upper body. It is thus natural to consider how to add an upper body to a passive-dynamic walker without destroying the passive dynamics. This problem was first discussed in McGeer's early study [2], and several studies considering passive dynamics on level dynamic walking with a torso have since been reported. Spong *et al.* studied a simple underactuated biped walker with a torso, but the center of mass (CoM) of all links was positioned at the hip joint [3]. Kinugasa *et al.* tried to realize passive dynamic walking (PDW) by applying PD control to a torso whose CoM was at the hip joint [4]. Narukawa *et al.* studied underactuated level dynamic walking with a torso stabilized through a PD control following McGeer's idea [5]. Sasaki and Yamakita investigated energy efficiency in virtual passive dynamic walking (VPDW) with a torso [6]. These studies reported that energy efficiency of dynamic walking grew worse as a result of adding a torso. This is mainly caused by joint torques to keep the torso upright under the influence of gravity. If the upper body could be *passively* stabilized to remain upright, this problem would be overcome. The answer is to be found in the use of a bisecting hip mechanism (BHM) [7][8]. A BHM is a mechanism to bisect the relative hip-joint angle with respect to the torso passively as shown in Fig. 1. Wisse *et al.* have already investigated PDW with a torso implementing a BHM [7] and realized experimental level dynamic walking [8]. However, they did not clarify the effect of the torso on the dynamic gait and driving mechanism at the CoM.

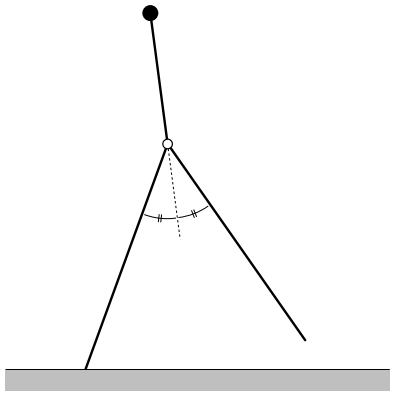

Fig. 1. Geometric relation between torso and legs according to bisecting hip mechanism

In this paper, we study the detailed mechanism, dynamics, and effects of BHM through mathematical modeling and numerical studies based on observations. We show that energy-efficient level dynamic bipedal walking can be achieved with a specific resistance of 0.01 [-] by utilizing the synergistic effect of BHM and the effect of semicircular feet. We then apply underactuated virtual passive dynamic walking (UVPDW) to generate energy-efficient dynamic gaits and confirm its validity in numerical simulations.

II. BISECTING HIP MECHANISM

This section describes the BHM and discusses its feasibility through development of a prototype.

Fig. 2 shows an overview of our prototype BHM. Although there are many approaches to realize a BHM, we did so with sprockets and chains. A sprocket is attached to the inner leg, and its rotational motion is inversely transmitted to another sprocket in the body through chains wound in the shape of the letter "S". One S chain loosens when the other stretches, so there exists a dead-band and backlash around the standing posture. The rotational motion of the sprocket is then transmitted forward to another one attached to the outer leg through another chain. The outer and inner legs then symmetrically move in opposite to each other with respect to the torso. Fig. 3 shows the symmetric motion of the legs. We can smoothly move two legs and maintain the posture at any angle. Back-drivability is almost completely achieved.

Although several dynamic walkers have already been developed [8][9], the effect of the upper body on the gait has not been theoretically clarified. The purpose of this paper is to understand the mechanism and dynamics in detail. In

F. Asano and Z.W. Luo are with the Bio-Mimetic Control Research Center, RIKEN, 463-0003 Nagoya, Japan {asano,luoz}@bmc.riken.jp
Z.W. Luo is also with the Department of Computer Science and Systems Engineering, Graduate School of Engineering, Kobe University luo@gold.kobe-u.ac.jp

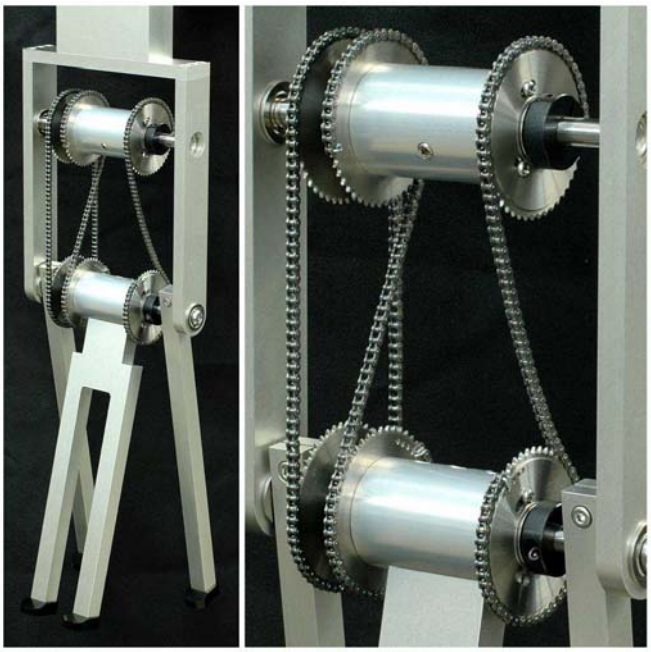

Fig. 2. Overview of prototype bisecting hip mechanism

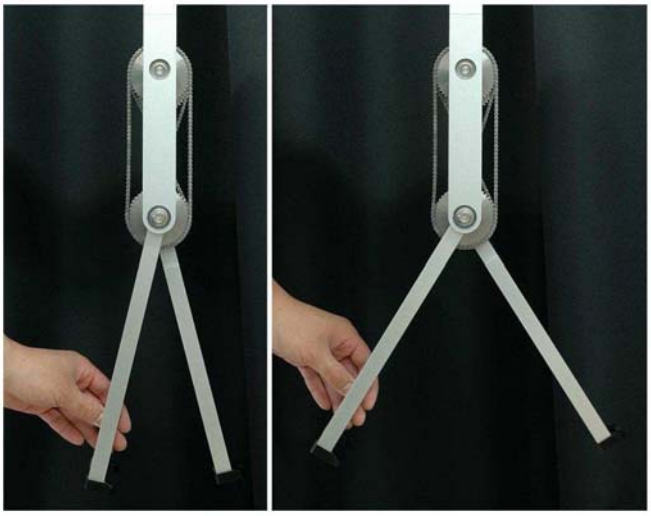

Fig. 3. Symmetric motion of legs

the following, we assume that the BHM does not have any friction and the back-drivability is perfect. We describe a simple biped model with a BHM and analyze the driving mechanism and dynamics.

III. MODELING OF UNDERACTUATED BIPED WALKING SYSTEM

This section describes the basic definitions and properties of the biped model.

A. Dynamic equation

We deal with a planar underactuated biped model with semicircular feet and a torso as shown in Fig. 4. We add a 1-link torso as the upper body to the biped incorporating a BHM. Its mass and inertia moment are m_T [kg] and I_T [kg·m^2]. The joint torques between the torso and stance-leg, u_1, and swing-leg, u_2, are known. The central point of

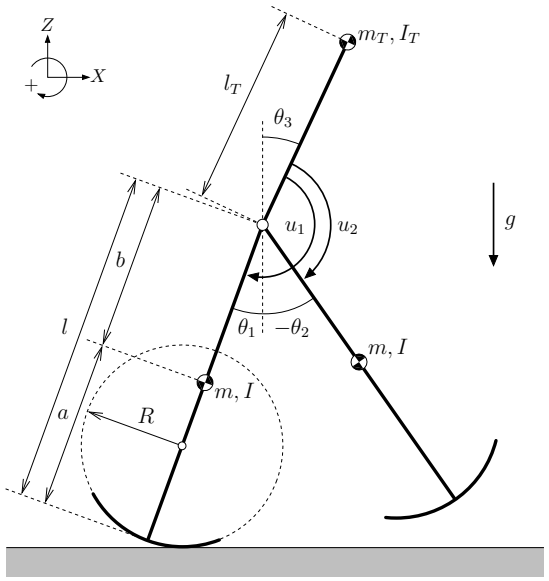

Fig. 4. Model of planar underactuated biped robot with semicircular feet and torso

the foot circle is positioned on the leg link, and the foot radius is R [m]. Let $\boldsymbol{\theta} = \begin{bmatrix} \theta_1 & \theta_2 & \theta_3 \end{bmatrix}^{\mathrm{T}}$ be the generalized coordinate vector; the dynamic equation of the biped model then becomes

$$\boldsymbol{M}(\boldsymbol{\theta})\ddot{\boldsymbol{\theta}} + \boldsymbol{h}(\boldsymbol{\theta}, \dot{\boldsymbol{\theta}}) = \boldsymbol{S}\boldsymbol{u} + \boldsymbol{J}_H^{\mathrm{T}}\lambda_H, \tag{1}$$

where $\boldsymbol{J}_H^{\mathrm{T}}\lambda_H \in \mathbb{R}^3$ denotes the constraint force vector caused by the BHM. The control input vector $\boldsymbol{S}\boldsymbol{u} \in \mathbb{R}^3$ is defined as

$$\boldsymbol{S}\boldsymbol{u} = \begin{bmatrix} 1 & 0 \\ 0 & 1 \\ -1 & -1 \end{bmatrix} \begin{bmatrix} u_1 \\ u_2 \end{bmatrix} \tag{2}$$

The geometric relation between the torso and legs according to the BHM is given by

$$\theta_3 = \frac{\theta_1 + \theta_2}{2} + \psi, \tag{3}$$

where ψ [rad] is the offset angle of the torso and is a constant. Fig. 5 shows the geometric relation. The time derivative of Eq. (3) is

$$\dot{\theta}_3 = \frac{\dot{\theta}_1 + \dot{\theta}_2}{2}. \tag{4}$$

This can be simply rearranged as

$$\boldsymbol{J}_H\dot{\boldsymbol{\theta}} = 0, \ \boldsymbol{J}_H = \begin{bmatrix} 1 & 1 & -2 \end{bmatrix}. \tag{5}$$

This leads to $\boldsymbol{J}_H\ddot{\boldsymbol{\theta}} = 0$, and by substituting this into Eq. (1), we obtain λ_H as

$$\lambda_H = -X_H(\boldsymbol{\theta})^{-1}\boldsymbol{J}_H\boldsymbol{M}(\boldsymbol{\theta})^{-1}\left(\boldsymbol{S}\boldsymbol{u} - \boldsymbol{h}(\boldsymbol{\theta}, \dot{\boldsymbol{\theta}})\right), \tag{6}$$

$$X_H(\boldsymbol{\theta}) = \boldsymbol{J}_H\boldsymbol{M}(\boldsymbol{\theta})^{-1}\boldsymbol{J}_H^{\mathrm{T}}. \tag{7}$$

By substituting this into Eq. (1), we further simplify the robot's dynamic equation to be

$$\boldsymbol{M}(\boldsymbol{\theta})\ddot{\boldsymbol{\theta}} = \boldsymbol{Y}_H(\boldsymbol{\theta})\left(\boldsymbol{S}\boldsymbol{u} - \boldsymbol{h}(\boldsymbol{\theta}, \dot{\boldsymbol{\theta}})\right), \tag{8}$$

where

$$\boldsymbol{Y}_H(\boldsymbol{\theta}) = \boldsymbol{I}_3 - X_H(\boldsymbol{\theta})^{-1}\boldsymbol{J}_H^{\mathrm{T}}\boldsymbol{J}_H\boldsymbol{M}(\boldsymbol{\theta})^{-1}. \tag{9}$$

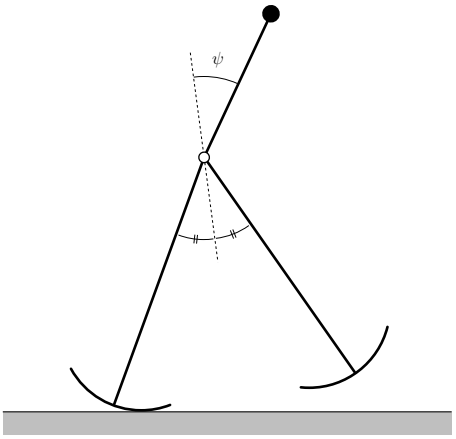

Fig. 5. Geometric relation of angular positions according to bisecting hip mechanism

B. Transition equation

The heel-strike is modeled as an inelastic collision. We introduce the extended coordinate vector, $\boldsymbol{q}_i \in \mathbb{R}^3$, for the two legs ($i = 1$ or 2) and torso ($i = 3$): $\boldsymbol{q}_i = \begin{bmatrix} x_i & z_i & \theta_i \end{bmatrix}^{\mathrm{T}}$. Fig. 6 shows the configuration at the instant of the heel-strike. The augmented coordinate vector is defined as $\boldsymbol{q} = \begin{bmatrix} \boldsymbol{q}_1^{\mathrm{T}} & \boldsymbol{q}_2^{\mathrm{T}} & \boldsymbol{q}_3^{\mathrm{T}} \end{bmatrix}^{\mathrm{T}}$, and the inelastic collision model is

$$\bar{\boldsymbol{M}}(\boldsymbol{q})\dot{\boldsymbol{q}}^{+} = \bar{\boldsymbol{M}}(\boldsymbol{q})\dot{\boldsymbol{q}}^{-} - \boldsymbol{J}_I(\boldsymbol{q})^{\mathrm{T}}\boldsymbol{\lambda}_I, \tag{10}$$

$$\boldsymbol{J}_I(\boldsymbol{q})\dot{\boldsymbol{q}}^{+} = \boldsymbol{0}_{7\times 1}, \tag{11}$$

where $\bar{\boldsymbol{M}} \in \mathbb{R}^{9\times 9}$ and $\boldsymbol{J}_I \in \mathbb{R}^{7\times 9}$. $\boldsymbol{\lambda}_I \in \mathbb{R}^7$ denotes the impact force on the robot. Eq. (11) implies the constraint condition of the post-impact velocities, and we describe the details in the following.

Leg 1's and Leg 2's hips are positioned the same as the Torso's, and their relations can be expressed as

$$x_1 + (l-R)\sin\theta_1 = x_3,\ z_1 + (l-R)\cos\theta_1 = z_3,$$
$$x_2 + (l-R)\sin\theta_2 = x_3,\ z_2 + (l-R)\cos\theta_2 = z_3.$$

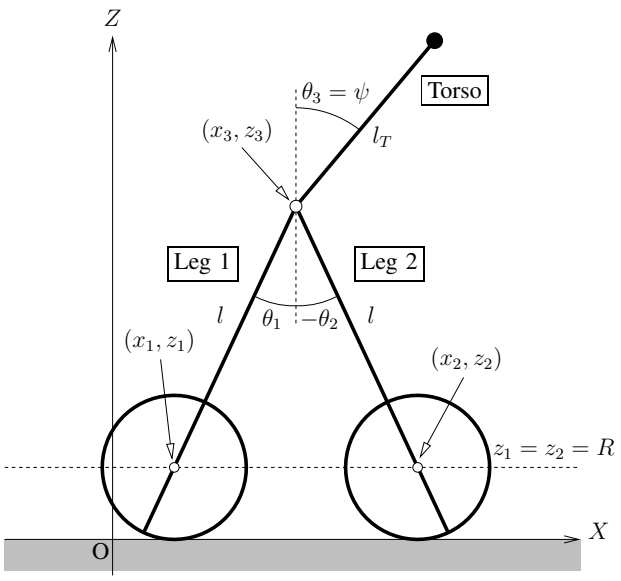

Fig. 6. Configuration at instant of heel-strike

Their time derivatives are

$$\dot{x}_1^{+} + (l-R)\dot{\theta}_1^{+}\cos\theta_1 = \dot{x}_3^{+}, \tag{12}$$

$$\dot{z}_1^{+} - (l-R)\dot{\theta}_1^{+}\sin\theta_1 = \dot{z}_3^{+}, \tag{13}$$

$$\dot{x}_2^{+} + (l-R)\dot{\theta}_2^{+}\cos\theta_2 = \dot{x}_3^{+}, \tag{14}$$

$$\dot{z}_2^{+} - (l-R)\dot{\theta}_2^{+}\sin\theta_2 = \dot{z}_3^{+}. \tag{15}$$

On the other hand, the conditions of rolling contact of Leg 2 with the ground are given by

$$\dot{x}_2^{+} = R\dot{\theta}_2^{+}, \tag{16}$$

$$\dot{z}_2^{+} = 0. \tag{17}$$

Furthermore, the constraint on the post-impact angular velocities due to the BHM is given by

$$\dot{\theta}_1^{+} + \dot{\theta}_2^{+} = 2\dot{\theta}_3^{+}. \tag{18}$$

The above seven conditions can be formulated as a matrix $\boldsymbol{J}_I$:

$$\boldsymbol{J}_I(\boldsymbol{q}) = \begin{bmatrix} 1 & 0 & J_{13} & 0 & 0 & 0 & -1 & 0 & 0 \\ 0 & 1 & J_{23} & 0 & 0 & 0 & 0 & -1 & 0 \\ 0 & 0 & 0 & 1 & 0 & J_{36} & -1 & 0 & 0 \\ 0 & 0 & 0 & 0 & 1 & J_{46} & -1 & 0 & 0 \\ 0 & 0 & 0 & 1 & 0 & -R & 0 & 0 & 0 \\ 0 & 0 & 0 & 0 & 1 & 0 & 0 & 0 & 0 \\ 0 & 0 & 1 & 0 & 0 & 1 & 0 & 0 & -2 \end{bmatrix}, \tag{19}$$

where

$$J_{13} = (l-R)\cos\theta_1, \quad J_{23} = -(l-R)\sin\theta_1,$$
$$J_{36} = (l-R)\cos\theta_2, \quad J_{46} = -(l-R)\sin\theta_2.$$

C. Mechanical energy

The robot's total mechanical energy is defined as the sum of kinetic and potential energies:

$$E(\boldsymbol{\theta}, \dot{\boldsymbol{\theta}}) = \frac{1}{2}\dot{\boldsymbol{\theta}}^{\mathrm{T}}\boldsymbol{M}(\boldsymbol{\theta})\dot{\boldsymbol{\theta}} + P(\boldsymbol{\theta}), \tag{20}$$

and its time derivative satisfies the following relation:

$$\dot{E} = \dot{\boldsymbol{\theta}}^{\mathrm{T}}\boldsymbol{S}\boldsymbol{u} = \left(\dot{\theta}_1 - \dot{\theta}_3\right)u_1 + \left(\dot{\theta}_2 - \dot{\theta}_3\right)u_2. \tag{21}$$

By using Eq. (4), this can be rearranged as

$$\dot{E} = \frac{\dot{\theta}_H u_1}{2} - \frac{\dot{\theta}_H u_2}{2}, \tag{22}$$

where $\theta_H := \theta_1 - \theta_2$ is the relative hip-joint angle.

D. Energy efficiency

The energy efficiency of a walking robot can be evaluated in terms of specific resistance $:= p/Mgv$ [-], which implies an expenditure of energy per unit mass and per unit length traveled. $M := m_T + 2m$ [kg] is the robot's total mass, and $g = 9.81$ [m/s^2] is the gravity acceleration. p [J/s] is the average input power defined as

$$p := \frac{1}{T}\int_{0^+}^{T^-} \frac{\left|\dot{\theta}_H u_1\right| + \left|\dot{\theta}_H u_2\right|}{2}\mathrm{d}t, \tag{23}$$

and v [m/s] is the average walking speed defined as

$$v := \frac{1}{T}\int_{0^+}^{T^-} \dot{X}_g\ \mathrm{d}t = \frac{\Delta X_g}{T}, \tag{24}$$

where T [s] is the steady step period, X_g [m] is the X-position of the center of mass (CoM), and $\Delta X_g := X_g(T^-) - X_g(0^+)$ [m] is the change in the CoM and is equal to the step.

IV. DYNAMIC ANALYSIS OF BIPED MODEL

This section derives the reduced walking model and analyzes the driving mechanism.

A. Driving mechanism and control input

We first derive the reduced walking model. Let $\bar{\boldsymbol{\theta}} = \begin{bmatrix} \theta_1 & \theta_2 \end{bmatrix}^{\mathrm{T}}$ be the generalized coordinate vector of the reduced walking system, the relation between this and the original coordinate vector, $\boldsymbol{\theta}$, is

$$\dot{\boldsymbol{\theta}} = \boldsymbol{T}\dot{\bar{\boldsymbol{\theta}}}, \quad \ddot{\boldsymbol{\theta}} = \boldsymbol{T}\ddot{\bar{\boldsymbol{\theta}}}, \quad \boldsymbol{T} = \begin{bmatrix} 1 & 0 \\ 0 & 1 \\ 1/2 & 1/2 \end{bmatrix}. \tag{25}$$

θ_3 can be eliminated by substituting Eq. (3), and using Eqs. (25), we can rearrange Eq. (1) as

$$\boldsymbol{M}(\bar{\boldsymbol{\theta}})\boldsymbol{T}\ddot{\bar{\boldsymbol{\theta}}} + \boldsymbol{h}(\bar{\boldsymbol{\theta}}, \dot{\bar{\boldsymbol{\theta}}}) = \boldsymbol{S}\boldsymbol{u} + \boldsymbol{J}_H^{\mathrm{T}}\lambda_H. \tag{26}$$

Here, note the relation,

$$\boldsymbol{J}_H^{\mathrm{T}} \in \mathrm{Ker}\left(\boldsymbol{T}^{\mathrm{T}}\right). \tag{27}$$

By multiplying both sides of Eq. (27) from the left by $\boldsymbol{T}^{\mathrm{T}}$, we obtain

$$\boldsymbol{T}^{\mathrm{T}}\boldsymbol{M}(\bar{\boldsymbol{\theta}})\boldsymbol{T}\ddot{\bar{\boldsymbol{\theta}}} + \boldsymbol{T}^{\mathrm{T}}\boldsymbol{h}(\bar{\boldsymbol{\theta}}, \dot{\bar{\boldsymbol{\theta}}}) = \boldsymbol{T}^{\mathrm{T}}\boldsymbol{S}\boldsymbol{u}. \tag{28}$$

We denote this system simply as

$$\boldsymbol{M}^{\sharp}(\bar{\boldsymbol{\theta}})\ddot{\bar{\boldsymbol{\theta}}} + \boldsymbol{h}^{\sharp}(\bar{\boldsymbol{\theta}}, \dot{\bar{\boldsymbol{\theta}}}) = \bar{\boldsymbol{S}}\boldsymbol{u}, \tag{29}$$

where $\boldsymbol{M}^{\sharp}(\bar{\boldsymbol{\theta}}) = \boldsymbol{T}^{\mathrm{T}}\boldsymbol{M}(\bar{\boldsymbol{\theta}})\boldsymbol{T} \in \mathbb{R}^{2\times 2}$, $\boldsymbol{h}^{\sharp}(\bar{\boldsymbol{\theta}}, \dot{\bar{\boldsymbol{\theta}}}) = \boldsymbol{T}^{\mathrm{T}}\boldsymbol{h}(\bar{\boldsymbol{\theta}}, \dot{\bar{\boldsymbol{\theta}}}) \in \mathbb{R}^2$, and $\boldsymbol{T}^{\mathrm{T}}\boldsymbol{S} = \bar{\boldsymbol{S}} \in \mathbb{R}^2$. The relation between the power and control inputs in the reduced walking system then becomes

$$\dot{E} = \dot{\bar{\boldsymbol{\theta}}}^{\mathrm{T}}\bar{\boldsymbol{S}}\boldsymbol{u} = \begin{bmatrix} \dot{\theta}_1 \\ \dot{\theta}_2 \end{bmatrix}^{\mathrm{T}} \begin{bmatrix} 1/2 & -1/2 \\ -1/2 & 1/2 \end{bmatrix} \begin{bmatrix} u_1 \\ u_2 \end{bmatrix}, \tag{30}$$

and the reduced control input vector is further simplified to

$$\bar{\boldsymbol{S}}\boldsymbol{u} = \begin{bmatrix} 1/2 \\ -1/2 \end{bmatrix}(u_1 - u_2). \tag{31}$$

Thus, we can find that each joint torque actuates the hip-joint alternately or these two control inputs are redundant actuations for one joint. This conclusion is also supported by Eq. (22).

B. Driving effects at CoM

We now analyze the driving mechanism of the joint-torque u_1 by transforming its effect into the translational force at the CoM, which is called generalized virtual gravity (GVG) [10]. This analysis pertains to a planar compass-like biped model without redundancy.

We set the contact point (ZMP) of the stance foot with the ground when $\theta_1 = 0$ as the origin O. The X-position of the ZMP then yields $R\theta_1$ [m]. Let $\bar{\boldsymbol{r}}_g \in \mathbb{R}^2$ be the positional vector of the reduced model's CoM, given by

$$\bar{\boldsymbol{r}}_g = \begin{bmatrix} X_g & Z_g \end{bmatrix}^{\mathrm{T}}, \tag{32}$$

$$MX_g = MR(\theta_1 - \sin\theta_1) + (m_T l + ma + ml)\sin\theta_1 - mb\sin\theta_2 + m_T l_T \sin\left(\frac{\theta_1+\theta_2}{2} + \psi\right), \tag{33}$$

$$MZ_g = MR(1 - \cos\theta_1) + (m_T l + ma + ml)\cos\theta_1 - mb\cos\theta_2 + m_T l_T \cos\left(\frac{\theta_1+\theta_2}{2} + \psi\right), \tag{34}$$

and its time derivative is

$$\dot{\bar{\boldsymbol{r}}}_g = \bar{\boldsymbol{J}}_g(\bar{\boldsymbol{\theta}})\dot{\bar{\boldsymbol{\theta}}} = \begin{bmatrix} J_{11} & J_{12} \\ J_{21} & J_{22} \end{bmatrix} \begin{bmatrix} \dot{\theta}_1 \\ \dot{\theta}_2 \end{bmatrix}, \tag{35}$$

where

$$MJ_{11} = MR(1 - \cos\theta_1) + (m_T l + ma + ml)\cos\theta_1 + \frac{m_T l_T}{2}\cos\left(\frac{\theta_1+\theta_2}{2} + \psi\right), \tag{36}$$

$$MJ_{12} = -mb\cos\theta_2 + \frac{m_T l_T}{2}\cos\left(\frac{\theta_1+\theta_2}{2} + \psi\right), \tag{37}$$

$$MJ_{21} = -MR\sin\theta_1 - (m_T l + ma + ml)\sin\theta_1 - \frac{m_T l_T}{2}\sin\left(\frac{\theta_1+\theta_2}{2} + \psi\right), \tag{38}$$

$$MJ_{22} = mb\sin\theta_2 - \frac{m_T l_T}{2}\sin\left(\frac{\theta_1+\theta_2}{2} + \psi\right). \tag{39}$$

By using the Jacobian matrix, $\bar{\boldsymbol{J}}_g(\bar{\boldsymbol{\theta}})$, the control input vector as an equivalent transformed torque of GVG can be expressed as $\bar{\boldsymbol{S}}\boldsymbol{u} = \bar{\boldsymbol{J}}_g(\bar{\boldsymbol{\theta}})^{\mathrm{T}}\boldsymbol{f}_g$. The inverse of $\bar{\boldsymbol{J}}_g$ can be derived and the GVG vector, $\boldsymbol{f}_g$, can be then obtained as

$$\boldsymbol{f}_g = \bar{\boldsymbol{J}}_g(\bar{\boldsymbol{\theta}})^{-\mathrm{T}}\bar{\boldsymbol{S}}\boldsymbol{u} = -\frac{1}{2\Delta_g}\left(\bar{\boldsymbol{r}}_g - \begin{bmatrix} R\theta_1 \\ 0 \end{bmatrix}\right), \tag{40}$$

where $\Delta_g := \det\left(\bar{\boldsymbol{J}}_g\right)$. This shows that the GVG yields a central force from the ZMP to CoM. As shown in Fig. 7, the GVG drives the CoM as a centripetal force during the first half cycle, and the rolling effect of the semicircular feet also drives the CoM as the virtual ankle-joint torque whose value is $-MRg\sin\theta_1$ [N·m] [10]. The robot can thus overcome the potential barrier at mid-stance, and after that, the GVG acts as a centrifugal force.

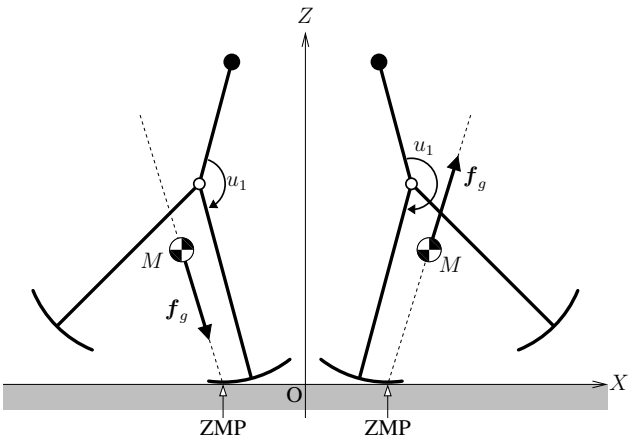

Fig. 7. Generalized virtual gravity mechanism

V. UNDERACTUATED VIRTUAL PASSIVE DYNAMIC WALKING

This section describes energy-efficient level walking through UVPDW. The walking system's performance with respect to the physical parameters of the torso is numerically analyzed.

A. Control law and typical gait

For simplicity, we assume $u_2 = 0$ and a UVPDW condition:

$$\dot{E} = \frac{\dot{\theta}_H u_1}{2} = Mg\tan\phi\dot{X}_g, \tag{41}$$

where ϕ [rad] is the virtual slope angle. u_1 is then uniquely determined as

$$u_1 = \frac{2Mg\tan\phi\dot{X}_g}{\dot{\theta}_H}. \tag{42}$$

This control input has a singularity at $\dot{\theta}_H = 0$, however, this singularity does not matter because the condition $\dot{\theta}_H > 0$ always holds during the stance phases as we later show. In the case of $u_1 = 0$, we obtain u_2 as

$$u_2 = -\frac{2Mg\tan\phi\dot{X}_g}{\dot{\theta}_H}, \tag{43}$$

and this generates the same dynamic gait as that generated by Eq. (42). For simplicity, we consider only the case of $u_2 = 0$ in the following.

Fig. 8 shows the typical gait of UVPDW where $\phi = 0.01$ [rad]. Here, (a) is the angular positions, (b) the angular velocities, (c) the control input (hip-joint torque), and (d) the mechanical energy. The physical parameters were chosen as in Table I. According to the UVPDW method, a stable dynamic gait was successfully generated by restoring the mechanical energy during the stance phases. Figs. 8 (a) and (b) indicates that the torso stays at the center between the two legs. This confirms the effect of Eqs. (3) and (4). Fig. 9 plots the stick diagram of one cycle, and we can see that the torso is passively stabilized to stay upright through the effect of the BHM.

Fig. 8 (b) shows that the singularity of $\dot{\theta}_H = 0$ is automatically avoided or that $\dot{\theta}_H > 0$ always holds during a cycle. This can be mathematically explained, but we leave the details for another paper. Through this effect, the control input does not diverge, and the maximum efficiency condition is achieved. Moreover, the specific resistance is

$$\frac{p}{Mgv} = \frac{\int_{0^+}^{T^-}\left(\dot{\theta}_H u_1/2\right)\mathrm{d}t/T}{Mg\Delta X_g/T} = \frac{Mg\tan\phi\Delta X_g}{Mg\Delta X_g} = \tan\phi.$$

Since we chose $\phi = 0.01$ [rad] in this case, the specific resistance is 0.01 [-].

TABLE I

PHYSICAL PARAMETERS OF BIPED ROBOT

m_T	5.0	kg
m	5.0	kg
I_T	0.001	kg·m^2
I	0.001	kg·m^2

l_T	0.3	m
$l\ (=a+b)$	1.0	m
a	0.5	m
b	0.5	m
R	0.3	m

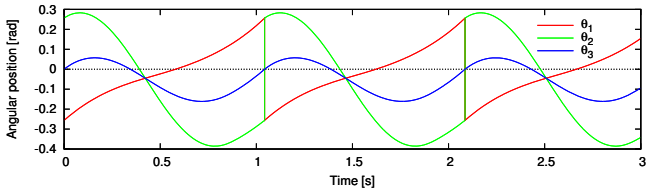

(a) Angular position

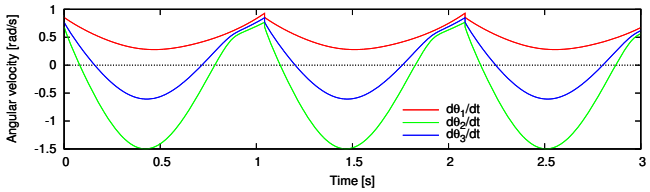

(b) Angular velocity

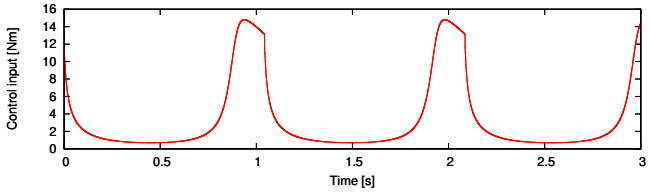

(c) Control input

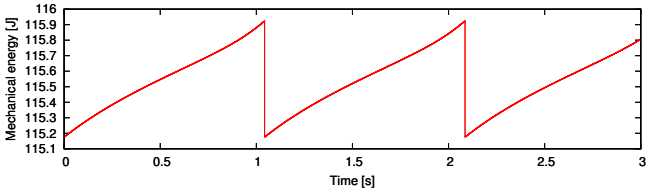

(d) Mechanical energy

Fig. 8. Simulation results for underactuated virtual passive dynamic walking

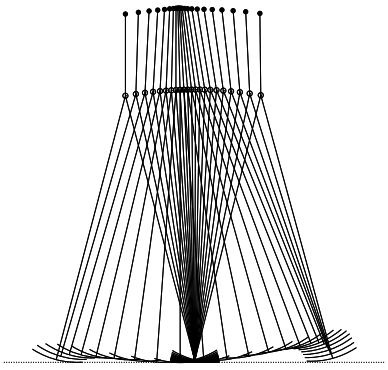

Fig. 9. Stick diagram of steady walking pattern

B. Parametric study

This subsection numerically investigates the effect of varying the physical parameters of the upper body. The specific resistance is kept constant (0.01 [-]) in all simulations, so its plots are omitted and only the walking speeds are evaluated. The physical parameters except the foot radius, R, were chosen as in Table I.

1) Effect of l_T: We first examine the effect of the torso length, l_T. Fig. 10 (a) plots the walking speed with respect to l_T for four values of R. There is a tendency that the walking speed monotonically decreases as l_T increases. This is because the upper body incorporating the BHM affects

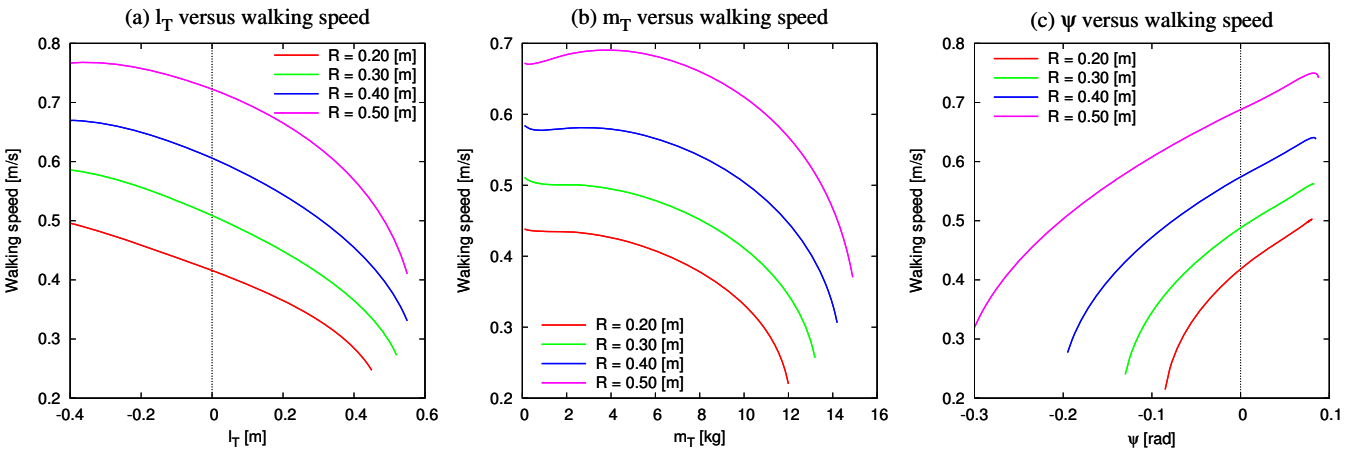

Fig. 10. Physical parameters of upper body versus walking speed for four values of R

as a counterweight and disrupts the leg-swinging motion, and this effect increases as the Z-position of the CoM, Z_g, becomes high. Also notice that the larger the foot radius is, the faster the walking speed becomes. This is because, as previously mentioned, a large foot radius drives the CoM forward more effectively and decreases mechanical energy loss caused by heel-strikes [11]. These effects can also be seen in the following two cases. Semicircular feet are advantageous because they increase energy efficiency and walking speed.

2) Effect of m_T: Next, we examine the effect of the torso mass, m_T. Fig. 10 (b) shows the walking speed with respect to m_T for four values of R. In this case, there is a tendency that the walking speed monotonically decreases as m_T increases. This can also be explained for the same reason as in the case of l_T; i.e., the larger m_T is, the higher Z_g becomes.

3) Effect of ψ: We finally examine the effect of the offset angle of the torso, ψ. Fig. 10 (c) shows the walking speed for four values of R. In all cases, the walking speed almost monotonically increases with ψ. This is because a forward-leaning posture causes forward acceleration or advantageous to overcome the potential barrier at mid-stance. Whereas for $\psi < 0$, a large foot radius, which produces large ankle-joint torque virtually, is required to cope with the backward acceleration. The results confirm that the stable range is wider in the case with large R.

VI. CONCLUSIONS AND FUTURE WORK

In this paper, we proposed an approach to energy-efficient dynamic bipedal locomotion with an upper body by means of a BHM and UVPDW. The driving mechanism was clarified, and the reduced walking system was easily dealt with as a simple compass-like biped without an upper body. The validity of the proposed method was confirmed in numerical simulations. Although we achieved our purpose, we have not investigated the utilization of the upper body dynamics yet.

Compared with humans, the stable range of the torso's physical parameters are not very wide. This is because UVPDW does not have any desired trajectories for stabilization in return for high energy efficiency. We should consider how to enlarge the stable domain without destroying the natural dynamics. We are currently developing a new walking machine with an upper body having a BHM and we will experimentally evaluate its gait features. The results of these experiments will be reported in a future paper.

VII. ACKNOWLEDGMENTS

This work was partially supported by a Grant-in-Aid for Scientific Research, (B) No. 18360115, provided by the Japan Society for the Promotion of Science (JSPS). The authors would like to thank ONO-DENKI CO., LTD. for many helpful suggestions and technical supports in development of the prototype bisecting hip mechanism.

REFERENCES

[1] T. McGeer, "Passive dynamic walking," *Int. J. of Robotics Research*, Vol. 9, No. 2, pp. 62–82, 1990.
[2] T. McGeer, "Dynamics and control of bipedal locomotion," *J. of Theoretical Biology*, Vol. 163, No. 3, pp. 277–314, 1993.
[3] M.W. Spong, R. Lozano and R. Mahony, "An almost linear biped," *Proc. of the IEEE Conf. on Decision and Control*, Vol. 5, pp. 4803–4808, 2000.
[4] T. Kinugasa, Y. Hashimoto and H. Fushimi, "Passive walking of biped Emu with attitude control of body," *Proc. of the IEEE/RSJ Int. Conf. on Intelligent Robots and Systems*, pp. 346–351, 2003.
[5] T. Narukawa, M. Takahashi and K. Yoshida: "Biped locomotion on level ground by torso and swing-leg control based on passive-dynamic walking," *Proc. of the IEEE/RSJ Int. Conf. on Intelligent Robots and Systems*, pp. 3431–3436, 2005.
[6] T. Sasaki and M. Yamakita, "Efficient walking control of robot with torso based on passive dynamic walking," *IEEE Int. Conf. on Mechatronics*, pp. TuA2-B-2(1)–TuA2-B-2(5), 2007.
[7] M. Wisse, A. L. Schwab and F. C. T. van der Helm: "Passive dynamic walking model with upper body," *Robotica*, Vol. 22, No. 6, pp. 681–688, 2004.
[8] M. Wisse, D. G. E. Hobbelen and A. L. Schwab: "Adding an upper body to passive dynamic walking robots by means of a bisecting hip mechanism," *IEEE Transactions on Robotics*, Vol. 23, No. 1, pp. 112–123, 2007.
[9] S. Collins, A. Ruina, R. Tedrake and M. Wisse: "Efficient bipedal robots based on passive dynamic walkers," *Science Magazine*, Vol. 307, No. 5712, pp. 1082–1085, 2005.
[10] F. Asano and Z.W. Luo, "Dynamic analyses of underactuated virtual passive dynamic walking," *Proc. of the IEEE Int. Conf. on Robotics and Automation*, pp. 3210–3217, 2007.
[11] F. Asano and Z.W. Luo, "The effect of semicircular feet on energy dissipation by heel-strike in dynamic biped locomotion," *Proc. of the IEEE Int. Conf. on Robotics and Automation*, pp. 3976–3981, 2007.